Journal of Science: Advanced Materials and Devices 7 (2022) 100417

Contents lists available at ScienceDirect

Journal of Science: Advanced Materials and Devices

journal homepage: www.elsevier.com/locate/jsamd

Original Article

ROS-responsive Ag-TiO_2 hybrid nanorods for enhanced photodynamic therapy of breast cancer and antimicrobial applications

Yike Hou [a, b, 1], Asim Mushtaq [a, b, 1], Zhe Tang [a, b], Eithne Dempsey [c], Yuling Wu [a, b], Yuguang Lu [a, b], Cong Tian [a, b], Jabeen Farheen [a, b], Xiangdong Kong [a, b, **], M. Zubair Iqbal [a, b, *]

[a] Institute of Smart Biomedical Materials, School of Materials Science and Engineering, Zhejiang Sci-Tech University, Hangzhou 310018, PR China
[b] Zhejiang-Mauritius Joint Research Center for Biomaterials and Tissue Engineering, Zhejiang Sci-Tech University, Hangzhou 310018, PR China
[c] Department of Chemistry, Kathleen Lonsdale Institute for Human Heath Research, Maynooth University, Maynooth, Ireland

ARTICLE INFO

Article history:
Received 13 September 2021
Received in revised form
16 December 2021
Accepted 5 January 2022
Available online 10 January 2022

Keywords:
Hybrid nanostructures
Silver-Titanium dioxide composites
Nanorods
Heterogeneous structure
Photodynamic therapy
Antimicrobial agent

ABSTRACT

There has been significant interest in designing heterostructured nanoparticles with excellent synergistic properties and multifunctionality. Herein, this work reports on the design of reactive oxygen species-(ROS-) responsive Ag decorated TiO_2 hybrid nanorods (HNRs) with dual functionalities of enhanced photodynamic therapy and antibacterial activity. A de-wetting phenomenon was employed to nucleate and crystallize Ag nanoparticles onto the surface of TiO_2 nanorods resulting in Ag-TiO_2 hybrid nanocomposites. The use of the Pluronic® F-127 polymer, which is permitted by the Food and Drug Administration (FDA), remarkably improved the biocompatibility of Ag-TiO_2 HNRs tested in 4T1 breast cancer cells. Furthermore, Ag-TiO_2 HNRs endocytosed by cancer cells produced high intracellular ROS under UV conditions (5.6 mW cm^{-2}), resulting in cancer cell apoptosis. Similarly, the distinctive features of Ag NPs on TiO_2 nanorods slow down the recombination rate of electrons−holes, and exhibited 90% killing efficacy against *Escherichia coli* (gram-negative/rods) and *Staphylococcus aureus* (gram-positive/cocci). The potential of photo-activated Ag-TiO_2 HNRs, as demonstrated in this work, indicates that this heterostructured material is a promising novel dual-therapeutic strategy against cancer cells and microbial agents.

1. Introduction

Amongst cancer therapies, photodynamic therapy (PDT) has been considered to be a non-invasive, auspicious, and clinically approved treatment approach that overcomes the shortcomings of other traditional anticancer therapies like chemotherapy and radiation therapy [1]. In PDT, the photosensitizer (PS) is a key player. First, the PS is locally or systemically administered into the desired area, and then a laser with a specific wavelength is used to irradiate the target tumor [2]. The administrated PS generates reactive oxygen species (ROS) after irradiation with subsequent cell death. However, traditional PSs are based on organic macro-molecules that have a rapid circulation time in the body with low efficiency under exposure to light [3,4]. Therefore, to improve the limitations of traditional PSs, inorganic TiO_2 nanoparticles have been of interest since they have shown great potential in applications to nanomedicine and environmental science [5]. Moreover, it is believed that the size and shape of TiO_2 particles have a notable influence on their photocatalytic properties [6]. Generally, small-sized nanoparticles present a large surface area that is beneficial for light absorption properties, resulting in an enhancement of photocatalytic performance [7]. Results revealed that a particle size *ca.* 25−40 nm was optimal for TiO_2 photocatalytic activity [8]. TiO_2 NPs with ~3.2-eV energy bandgaps can be activated with ultraviolet (UV) light and undergo electron transfer reactions followed by photogenerated electron holes. As a result, multiple ROSs are

* Corresponding author. Institute of Smart Biomedical Materials, School of Materials Science and Engineering, Zhejiang Sci-Tech University, Hangzhou 310018, PR China.
** Corresponding author. Zhejiang-Mauritius Joint Research Center for Biomaterials and Tissue Engineering, Zhejiang Sci-Tech University, Hangzhou 310018, PR China.,
E-mail addresses: kongxd@zstu.edu.cn (X. Kong), zubair@zstu.edu.cn (M.Z. Iqbal).
Peer review under responsibility of Vietnam National University, Hanoi.
[1] These authors contributed equally.

https://doi.org/10.1016/j.jsamd.2022.100417

generated, e.g., hydroxyl (HO·) and superoxide radical (O^{2-}), which then react with biological molecules such as phospholipids of the cellular membrane, macromolecules, DNA, and proteins resulting in tumor ablation [9–12]. However, studies have demonstrated a requirement for high intensity UV or visible light to activate PSs, thus hindering the practical therapeutic applications of TiO_2 NPs [13]. Interestingly, TiO_2 nanorod-shaped structures were shown to exhibit enhanced photocatalytic properties due to high surface area as compared with TiO_2 nanoparticles [14,15]. Therefore, it is necessary to design biocompatible nanocomposite-based materials with multifunctional characteristics that can possess the required properties under low light intensity conditions.

Furthermore, bacterial infections (particularly those that are antibiotic resistant) continue to be a global concern with respect to public health, clean potable water supplies, and food contamination [16]. Reports have revealed that microbial activity and bacterial infections cause the death of about 3 million people annually in developing countries [17]. Due to the excessive use of antibiotics, antimicrobial resistance has been a driver for research endeavors that include various metals-based nanoparticles in relation to new antimicrobial agents [18]. Amongst these, Ag has attained noteworthy attraction as an antibacterial agent due to low toxicity and biocompatibility [19]. Indeed, hypertoxic Ag^{+} ions are released in an oxidizing environment when Ag NPs are irradiated by an external source of light, which results in efficiently inhibited tumor and bacterial growth [20]. Recent studies confirmed that the antimicrobial properties of Ag NPs are profoundly superior to Cu and Au NPs [21,22]. In addition, ultra-small (5 nm) Ag NPs demonstrated excellent antibacterial effects as compared to large-sized nanoparticles, regardless of their shape, due to their high surface area. In addition, particles with high surface areas possessed faster dissolution rates when compared to those with smaller surface areas [23]. Further, the inhibition of microbes and the controlled interaction of NPs and bacteria can be achieved by doped hybrid nanostructures. These unique materials have attained significant attention recently as the next generation "smart nanorobots" owing to their multifunctional properties with a wide range of applications. These versatile structures consist of multiple components with various functionalities in a single entity to address the abovementioned challenges in PDT and antimicrobial action [24–26]. In addition, control over homogeneous size and shape and the biocompatibility of nanocomposites are currently under investigation.

In this work, a facile synthesis method was used to prepare Ag-TiO_2 nanorods where Ag NPs placed on the surface of TiO_2 nanorods slow down the recombination of electron–hole pairs resulting in enhanced photocatalytic activity. This, in turn, produces enough reactive oxygen species to destroy the cancerous cells and bacterial strains under study. The growth mechanism, cytotoxicity, ROS generation, *in vitro* PDT under low-power UV irradiation (5.6 mW cm^{-2}), and antimicrobial properties of the prepared Ag-TiO_2 hybrid nanorods (HNRs) are investigated in this work and discussed in detail. A schematic of the ROS-responsive Ag-TiO_2 hybrid nanorods for enhanced photodynamic therapy of breast cancer and antimicrobial applications are illustrated in Scheme 1.

2. Experimental

2.1. Synthesis of Ag-TiO_2 hybrid nanorods (HNRs)

TiO_2 nanorods were fabricated with a hydrothermal approach. Firstly, a mixture of 3.5 g, 3.3 g, and 2.3 g of oleic acid, oleyl amine, and ethanol, respectively, was prepared and then 3.4 g of titanium (IV) *butoxide* dissolved using stirring to obtain homogeneous solution. Subsequently, the above solution was transferred into a 20-mL Teflon tube and placed into another 100-mL Teflon tube providing an atmosphere of water and ethanol with a 1:2.5 ratio. The solution was sealed into a stainless steel autoclave and placed in an oven at 180 °C for 18 h. After the reaction solution was cooled down to room temperature, the sample was washed twice with ethanol and the product was obtained by centrifugation. Finally, the resulting TiO_2 material was dissolved in a non-polar solvent such as cyclohexane (10 mL). To grow the Ag nanoparticles on the TiO_2 nanorods, a thermal decomposition method was employed. A homogeneous solution was prepared by mixing 50 mg of silver nitrate ($AgNO_3$), oleyl amine (1 mL), and 4-*tert*-butyltoluene (20 mL) using 10 min of sonication. Then, the TiO_2 (1 mL) prepared in cyclohexane was poured into the above-mentioned homogeneous mixture and heated at 120 °C for 45 min under a nitrogen atmosphere. The Ag-TiO_2 nanoparticles were stabilized and dispersed in cyclohexane (10 mL) after washing three times with the mixture of ethanol and acetone. Finally, the FDA-approved triblock copolymer Pluronic® F-127 was used to change the phase of the prepared materials from organic to an aqueous solution [25]. Briefly, PF-127 (1 g) was dissolved in trichloromethane $CHCl_3$ (100 mL) before the addition of the Ag-TiO_2 HNRs (1 mL) from the stock solution and stirred for 4 h. Afterwards, water (10 mL) was added into the above solution to prepare an aqueous-organic emulsion. $CHCl_3$ was vaporized using a rotary evaporator. Finally, aqueous-dispersed HNRs were attained and washed twice with ethanol using centrifugation.

2.2. In vitro cell toxicity experiment

In order to evaluate the cytotoxicity of the aqueous dispersed Ag-TiO_2 HNRs, the colorimetric methyl thiazolyl tetrazolium (MTT) assay was employed. Particularly, 4T1 cells were seeded into a 96-well plate and cultured for 24 h in Dulbecco's modified eagle medium (DMEM, high glucose, GIBCO, C11995) supplemented with 10% fetal bovine serum (FBS, Thermo, SH3007003). Following this, the cells were incubated with PF-127-coated Ag-TiO_2 HNRs of different Ti concentrations (0, 20, 40, 80, and 100 μg/mL, diluted in DMEM) for 24 h at 37 °C under 5% CO_2. Then, the MTT solution (10 μL, 5 mg/mL) was added to each Bell and incubated for an additional 4 h before the addition of 100 μL of DMSO (Amresco, code 0231) for dissolution of the precipitate. Finally, a microplate reader (iMark 168–1130, Bio-rad, USA) with a wavelength of 480 nm was employed to measure the absorption of each well.

2.3. Detection of ROS generation

The ROS generation performance of the prepared Ag-TiO_2 HNRs was examined using the $^1O_2$ scavenger 1,3-Diphenylisobenzofuran (DPBF). Initially, DPBF was diluted with DMSO to a suitable concentration and then mixed with the HNRs. The absorbance of the DPBF-HNRs mixture was monitored by a UV-vis spectrophotometer before and after 5 min of UV irradiation.

2.4. In vitro photodynamic therapy

To evaluate the PDT effect of Ag-decorated TiO_2 hybrid nanorods on the 4T1 breast cancer cell line, the incubation time of HNRs was decreased to 4 h, and then the growth media was replaced with a fresh medium. The 4T1 breast cancer cells were incubated for a further 24 h after UV irradiation (0 min, 10 min, and 30 min). Following this, the MTT solution (10 μL, 5 mg/mL) was added to each well and incubated for another 4 h before the addition of 100 μL of DMSO (Amresco, code 0231) for dissolution of the precipitate. Finally, a microplate reader (iMark 168–1130, Bio-rad,

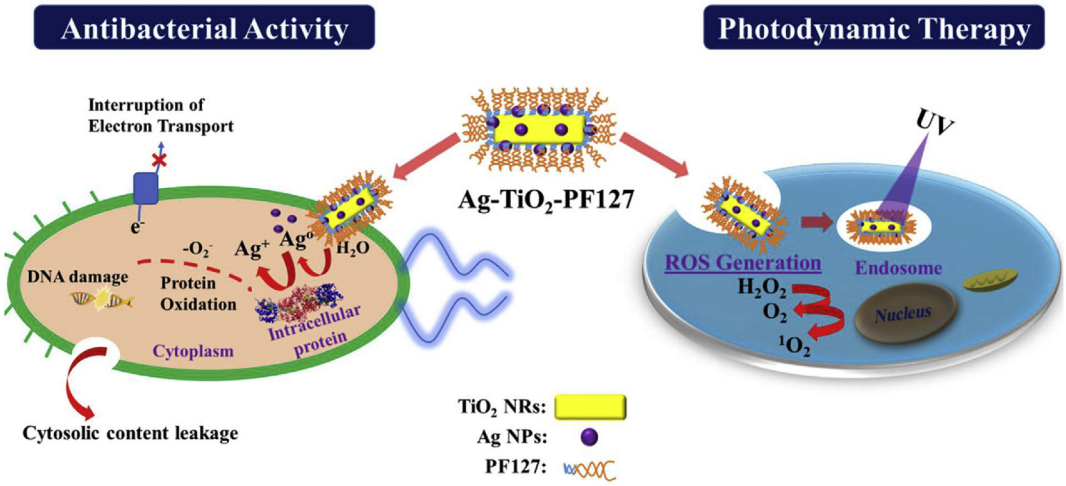

Scheme 1. A graphical representation of prepared Pluronic® F-127 coated Ag-TiO_2 HNRs for antibacterial and photodynamic therapy applications.

USA) with a wavelength of 550 nm was used to evaluate the absorbance of each well. For the qualitative assay, cytotoxicity was analyzed using a live/dead cytotoxicity kit (Mesgen Biotech, Shanghai, China). Briefly, various concentrations (0, 40, 80, and 120 μg/mL) of prepared Ag-TiO_2 HNRs were incubated with 4T1 cells for 12 h. Then the culture medium was substituted with fresh medium and exposed to UV light (5.6 mW cm^{-2}) for 0, 15, and 30 min. After incubation for another 4 h at 37 °C, the cells were stained for 30 min with Calcein AM and propidium iodide (PI). Finally, the live/dead cells were detected using a confocal scanning laser microscope (A1, Nikon, Japan) with excitation and emission of green (Calcein-AM, ex/em = 488/518 nm) and red (PI, ex/em = 535/615 nm) fluorescence.

2.5. Antibacterial activity testing

The antibacterial properties of the prepared TiO_2 and Ag-TiO_2 HNRs were investigated using *Escherichia coli* (gram-negative rods) and *Staphylococcus aureus* (gram-positive cocci). A monocolony of *E. coli* and *S. aureus* on a Luria–Bertani (LB) agar plate were separately transferred into two 10-mL LB culture media and grown at 37 °C for 12 h. The cultures were diluted with LB culture medium to adjust the OD at 600 nm to 0.1 AU (1×10^7 CFU/mL). Then the bacteria were diluted 10 times with LB to obtain the desired concentration of 1×10^6 colony forming units (CFU/mL). The synthesized TiO_2 and Ag-TiO_2 HNRs (500 μg/mL) were incubated with the bacterial culture (100 μL) and 800 μL of Luria broth for 6 h in a shaking incubator (37 °C, 160 rpm). Control experiments were carried out in parallel with the same conditions using phosphate-buffered saline (PBS). All measurements were carried out with n = 4 trials. Finally, 100 μL of each of the cultured samples was added into a 96-well plate and the optical density was read at 600 nm using a microplate reader.

2.6. Characterization

X-ray diffraction patterns (XRD) were made using a D8 Focus Powders diffractometer (Bruker) with Cu Kα radiation (λ = 0.154 nm). Structural characterizations were investigated by transmission electron microscopy (TEM), high-resolution TEM (HRTEM), and energy dispersive analysis (EDS) using a JEOL-2100 electron microscope. The zeta potential was tested on a Zetasizer Nanoseries (Nano-ZS, Malvern Instruments). Inductively-coupled plasma mass spectrometry (ICP-MS) was performed with an Optima 2100 instrument from PerkinElmer. X-ray photoelectron spectroscopy (XPS) was carried out on a Thermo Fisher Scientific K-ALPHA System.

3. Results and discussion

Comparative crystallographic studies were conducted in order to observe the purity of the prepared materials and the influence of Ag NPs on TiO_2. The diffraction pattern for TiO_2 and Ag-TiO_2 are shown in Fig. 1(a). Diffraction spectra corresponding to TiO_2 and Ag-TiO_2 HNRs is well-indexed to the tetragonal anatase structure with lattice parameters of a = b = 3.785 Å, c = 9.514 Å and $\alpha = \beta = \gamma = 90°$ (JCPDS file No.21-1272). The planes (101) (004), and (200) showed the crystallinity of the prepared TiO_2 NRs. However, the crystal intensity decreased in Ag-TiO_2 HNRs and some planes such as (105) and (211) merged into a single plane. In addition, the plane (102) at *ca.* 30° was not evident in the XRD of Ag-TiO_2 HNRs. Furthermore, some diffraction planes of Ag, such as (111) (142) and (220), were not apparent because these planes overlap with the (004) (211) and (204) diffraction planes of TiO_2, respectively [27]. From the XRD results, it is obvious that a low amount of Ag (ultra-small Ag NPs) did not influence the anatase crystalline phase but did disturb the crystallinity of the nanoparticles as Ag NPs present at the surface of TiO_2 [28,29].

Furthermore, in order to confirm the existence of Ag in the synthesized material, energy-dispersive spectroscopy (EDS) was conducted as shown in Fig. 1(b). The EDS spectra showed Ag peaks clearly visible in the spectrum. The strong copper peak (Cu) came from the TEM copper grid used as the sample holder.

A structural investigation such as the shape and size of the synthesized materials was performed using TEM. The low magnification image (Fig. 2a) illustrates the homogeneous shape and size of the TiO_2 nanorods. Furthermore, the obvious growth of ultra-small Ag nanoparticles can be seen on the TiO_2 nanorods and all the Ag nanoparticles were deposited on the surface of the nanorods (Fig. 2b) establishing a heterogeneous structure. Finally, the high resolution HR-TEM image presents a single Ag NP-TiO_2 nanorod structure and it can be seen that the size of the spherical Ag nanoparticle is about 4 ± 1 nm whereas the size of the individual nanorod is about 35 ± 5 nm in length and 13 ± 2 nm in width. HR-TEM scanning reveals lattice spacing values of 0.354 nm and 0.231 nm, which are incorporated with the interplanar spacing planes of (101) and (111) in the TiO_2 and Ag structure, respectively.

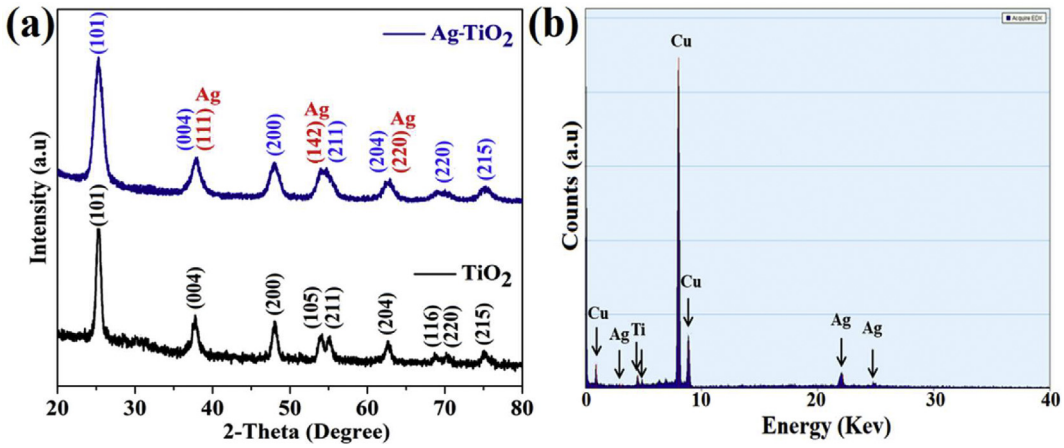

Fig. 1. (a) XRD pattern of the prepared TiO_2 and Ag-TiO_2 HNRs and (b) EDS spectra of Ag-TiO_2 hybrid nanorods.

As the sizes of the Ag nanoparticles are very small, they do not have sufficient ability to alter the dominant phase of TiO_2 as demonstrated in the XRD spectra. The distribution of size and dimensions, including width and size of prepared Ag-TiO_2 HNRs, were analyzed using the digital image processing software ImageJ from TEM images as shown in the Supporting Information (Figure S1(a, b)). The growth mechanism of Ag-TiO_2 hybrid nanorods is presented in Fig. 2d. In this facile synthesis route, the hydrothermally-prepared TiO_2 nanorods were mixed with a homogeneous solution containing silver precursor along with oleyl amine and TBT. The nanorods were fully dispersed inside the solution and, over time, the Ag precursor formed unstructured shells around the nanorods. As it is well known that temperature and time are pivotal parameters that affect crystal growth, by increasing the reaction parameters, the lattice mismatch between TiO_2 and Ag will become enhanced, and the shell starts to rupture. At a certain limit, the Ag shells nucleate and anneal at different positions on the surface of nanorods forming Ag spherical nanoparticles in a process called dewetting. Furthermore, Pluronic® F-127, an FDA-approved triblock polymer, was employed for surface modification of the prepared nanoparticles thus improving biocompatibility and phase transfer from hydrophobic to aqueous media. The zeta potential of uncoated HNRs and Pluronic® F-127-coated HNRs was assessed to understand the surface charge. Figure S1(c) demonstrates that PF127-modified NPs have +6 mV surface potential and bare HNRs have −10 mV, which indicates successful surface modification.

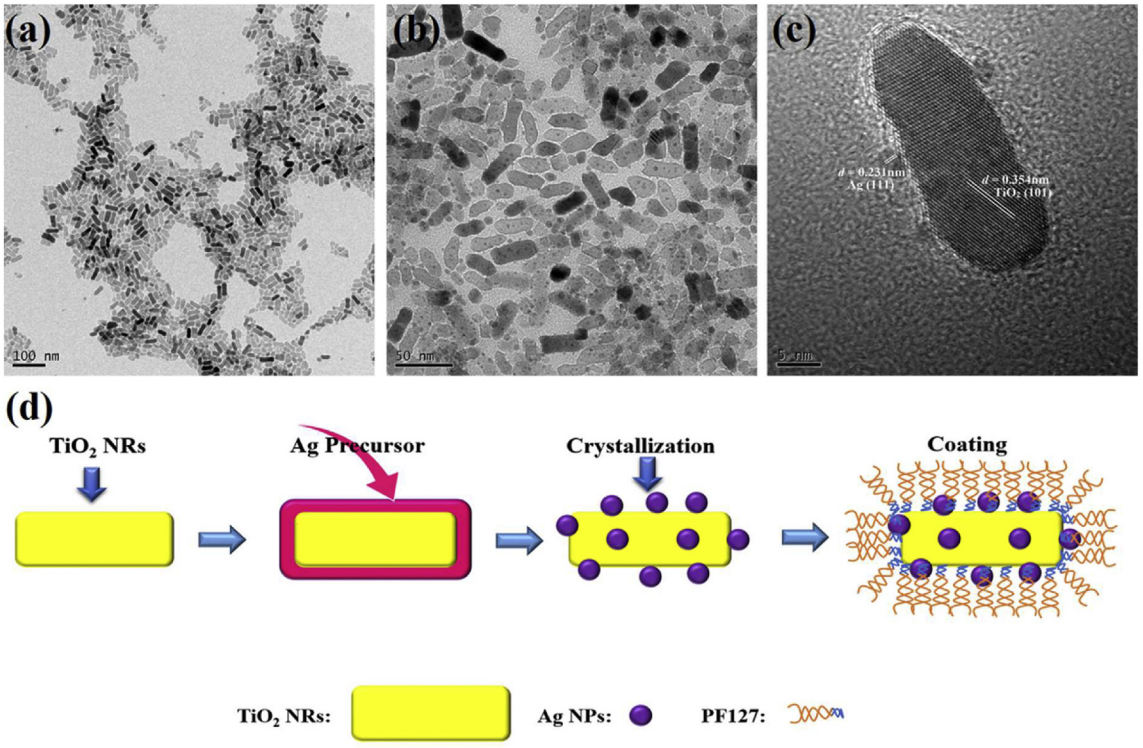

Fig. 2. (a) Transmission electron microscope images of TiO_2 nanorods (b, c) TEM and high resolution TEM images of Ag-TiO_2 hybrid nanorods, and (d) graphical representation of possible growth mechanism of hybrid nanorods.

In addition to structural characterization, x-ray photoelectron spectroscopy was employed to further confirm the states and surface components of Ag, Ti, and O in the Ag-TiO_2 HNRs. Fig. 3(a) reveals two significant XPS peaks at 368.0 eV and 373.9 eV, which are assigned to Ag ($3d_{5/2}$) and Ag ($3d_{3/2}$), respectively. The difference between these two binding energies is about 6 eV indicating the purity of the Ag NPs located on the surface of TiO_2 nanorods as Ag (0) metallic in nature. Fig. 3b also shows two sharp peaks at 458.8 eV

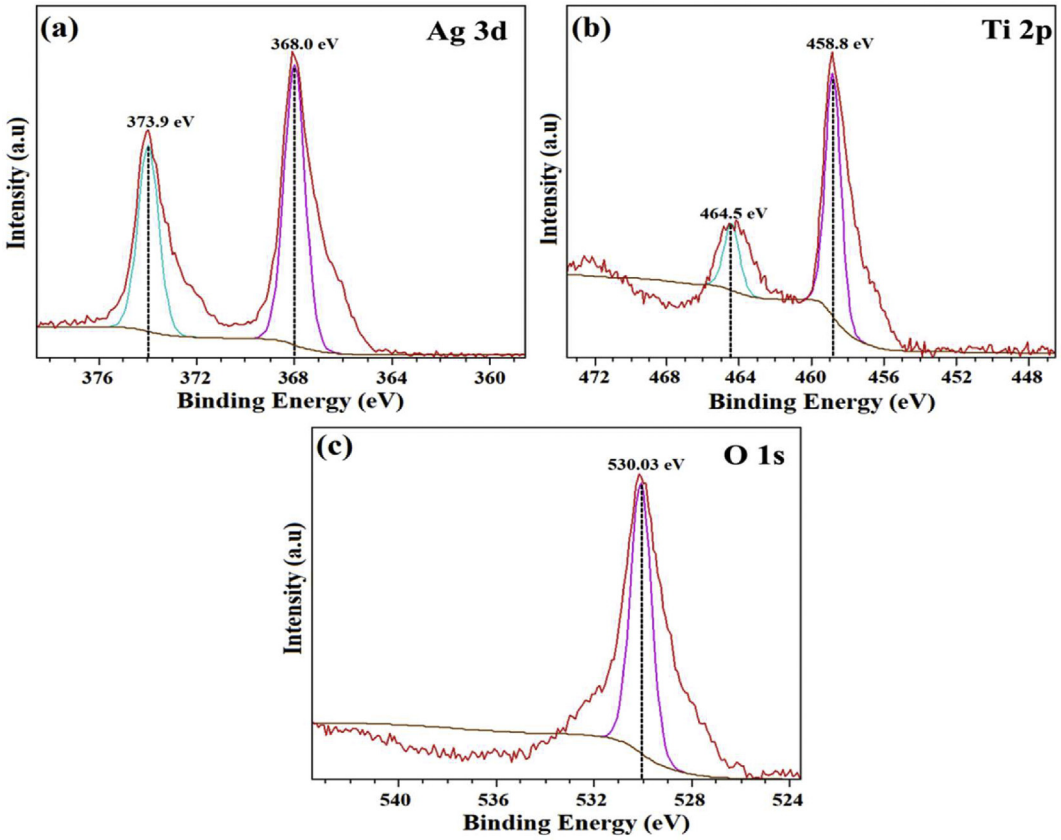

Fig. 3. Quantitative XPS analysis of (a) Ag 3d spectra of Ag NPs, (b) Ti 2p spectra of Ti, and (c) O 1s spectra of O.

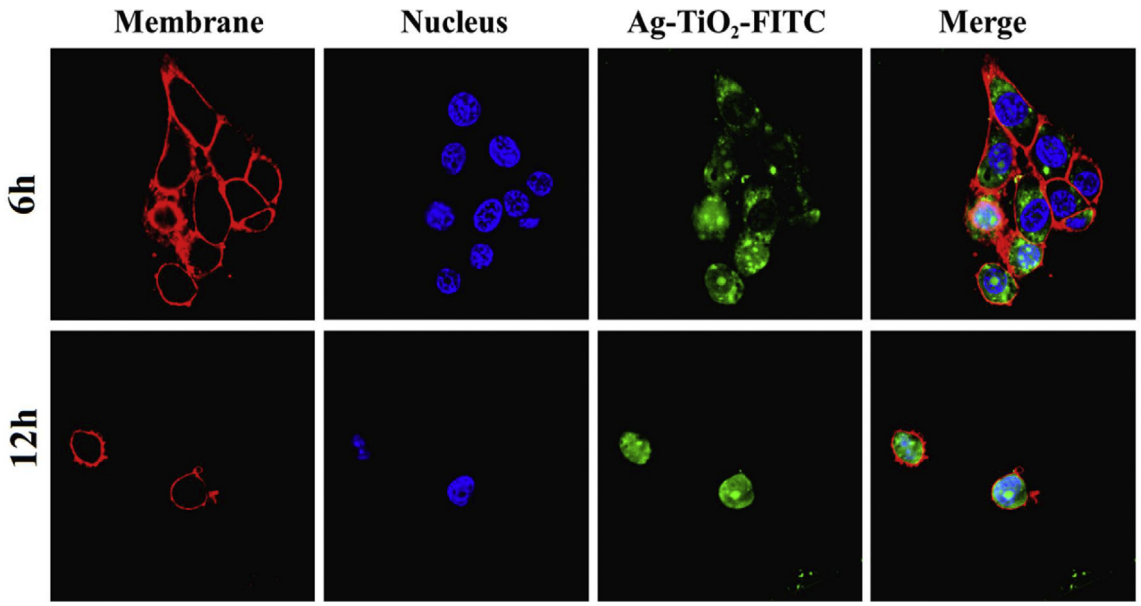

Fig. 4. Confocal photomicrographs of 4T1 after 6 and 12 h of co-incubation with Ag-TiO_2@PF127, which was labeled with FITC (green), the cell membrane labeled with Dil stain (red cell membrane probe), and nuclei were dyed by DAPI (blue).

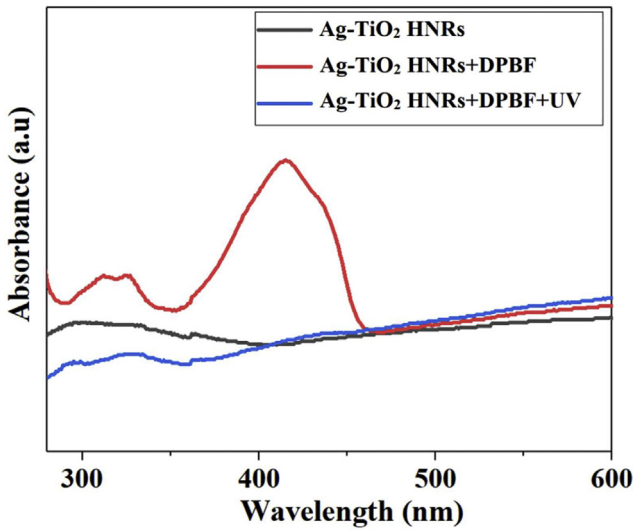

Fig. 5. UV-vis absorption spectra of PF-127-coated Ag-TiO_2 HNRs and DPBF coupled with Ag-TiO_2 HNRs with and without UV irradiation.

and 464.5 eV corresponding to Ti ($2p_{3/2}$) and Ti ($2p_{1/2}$), respectively, which are assigned to Ti^{4+} in TiO_2 with a difference of 5.7 eV. Moreover, the binding energy at 530.03 eV was attributed to O 1s (lattice oxygen atom, Ti—O) as shown in Fig. 3(c). The XPS spectra of Ag, Ti, and O are consistent with previous reports [30—32].

Fluorescence techniques are useful in materials science and biology because they enable visualization of in-depth information with respect to cell—nanoparticle interactions. Fluorescent nanoparticles can be easily monitored inside individual cells with high resolution [33]. Cellular uptake studies are also crucial for understanding the efficacy of drugs in photodynamic therapy [34]. Therefore, FITC (an organic fluorophore) was employed with synthesized Ag-TiO_2 HNRs to assess cellular uptake. The CLSM images in Fig. 4 showed that FITC-labeled Ag-TiO_2 HNRs were internalized into 4T1 cancer cells and mainly distributed in the cytoplasm within 6 h. Remarkably, the HNRs were completely taken up by cells within 12 h (Fig. 4) demonstrating that the nanomaterials are promising for drug delivery and therapeutic action. This high intracellular localization is associated with the positive charge of the HNRs (+6 eV zeta potential as given in Figure S1 of the Supporting Information) via electrostatic attractions [35].

Subsequently, the ROS generation detection study was necessary to reveal the therapeutic success rate following excellent cellular uptake. In this experiment, 1,3-Diphenylisobenzofuran (DPBF) was selected as a probe to investigate the ROS generation capability of the prepared Ag-TiO_2 NPs following UV irradiation. DPBF is a common ROS quencher, which reacts irreversibly with ROSs produced by photosensitizers resulting in a decrease in absorption of the DPBF at 415 nm [36]. Fig. 5 shows that the absorption of the Ag-TiO_2 HNRs slightly moved from the ultraviolet to visible region because of localized surface plasmon resonance (LSPR) of the Ag nanoparticles present on the surface of the TiO_2 NRs [37]. The hybrid nanorods combined with DPBF exhibited a prominent absorption peak at 415 nm corresponding to the DPBF. However, significant degradation of DPBF was observed after UV irradiation (5 min), which demonstrated a high level of ROS generation. Overall, the optimum cellular uptake and ROS generation shown here provides experimental evidence of the potential of these Ag-TiO_2@PF127 HNRs for biomedical phototherapeutic applications.

Cytotoxicity assessment is an important factor to assess the prospective applications of nanoparticles in clinics. Therefore, the cell viability of Ag-TiO_2 HNRs was examined using the MTT assay. Fig. 6 (a) illustrates the toxic impact of the HNRs on 4T1 cells incubated at various concentrations for 24 h. As understood from toxicity analysis, the HNRs showed a non-toxic effect at high concentration and more than 85% of cells were viable upon incubation with 100 μg/mL Ag-TiO_2 resulting in evidence of low cytotoxicity at this level.

In addition, the photo killing efficiency of the designed Ag-TiO_2 HNRs was assessed by MTT assay after using UV light as an external stimuli irradiation source. No obvious phototoxic effect on cancer cells was observed in the control groups, i.e., groups without HNRs and HNRs without UV irradiation. Fig. 6(b) shows that photodynamic therapeutic efficacy strongly depended on the concentration of Ag-TiO_2 HNRs and UV exposure time. Negligible phototoxic effects were determined at low concentration. However, over 90% cell death was recorded when the HNRs with 120 μg mL^{-1} concentration were irradiated with 30 min of UV light at low intensity (5.6 mW cm^{-2}), which demonstrates the high PDT efficacy of the as-prepared Ag-TiO_2 HNRs. Moreover, confocal scanning laser microscopy images of 4T1 breast cancer cells stained with propidium iodide (PI) and Calcein AM were recorded to intuitively verify the *in vitro* PDT efficiency. After PDT, live/dead cells were distinguished by Calcein AM (live cells, green fluorescence) and PI (dead cells, red fluorescence) as shown in Fig. 6(c). Green fluorescence was observed in the control group, i.e., only UV irradiation and HNRs without UV irradiation, suggesting that UV alone is harmless to cancerous cells at 5.6 mW cm^{-2} intensity. However, the red fluorescence (dead cells) was remarkably enhanced as the UV exposure time and concentration of HNRs increased and all cancer cells were killed at 120 μg mL^{-1} (30 min), which reveals a high rate of apoptosis. Therefore, according to the above results, as-prepared Ag-TiO_2 HNRs demonstrated the ability to generate $^1O_2$, which led to cell ablation during *in vitro* UV irradiation.

Lastly, the antibacterial performance of TiO_2 NRs and Ag-TiO_2 HNRs was investigated by evaluating the growth/viability of gram-negative *E. coli* and gram-positive *S. aureus* bacteria as model microbes. The bacteria survival percentage was assessed by measuring the optical density at 600 nm (OD_{600}) after incubation with the nanomaterials for a period of 6 h. As illustrated in Fig. 7(a and b), the TiO_2 NRs showed negligible inhibition capability and the survival rate was about 80%. However, the prepared Ag-TiO_2 HNRs exhibited remarkable inhibition of *E. coli* and *S. aureus* bacteria. Indeed, Ag-TiO_2 HNRs demonstrated prominent effects on gram-negative bacteria as gram-negative bacteria contained less peptidoglycan resulting in more silver particles or ions on the wall of the bacterial membrane. The Ag NPs damage the proteins and deactivate bacterial metabolism leading to ROS and oxidative stress [38,39]. Hence, this outstanding bacteria growth inhibition performance is due to the synergistic effect of the hybrid materials. In addition, Ag NPs present on the surface of the TiO_2 NRs slow down the recombination rate of electrons—holes, which also enhances antibacterial properties.

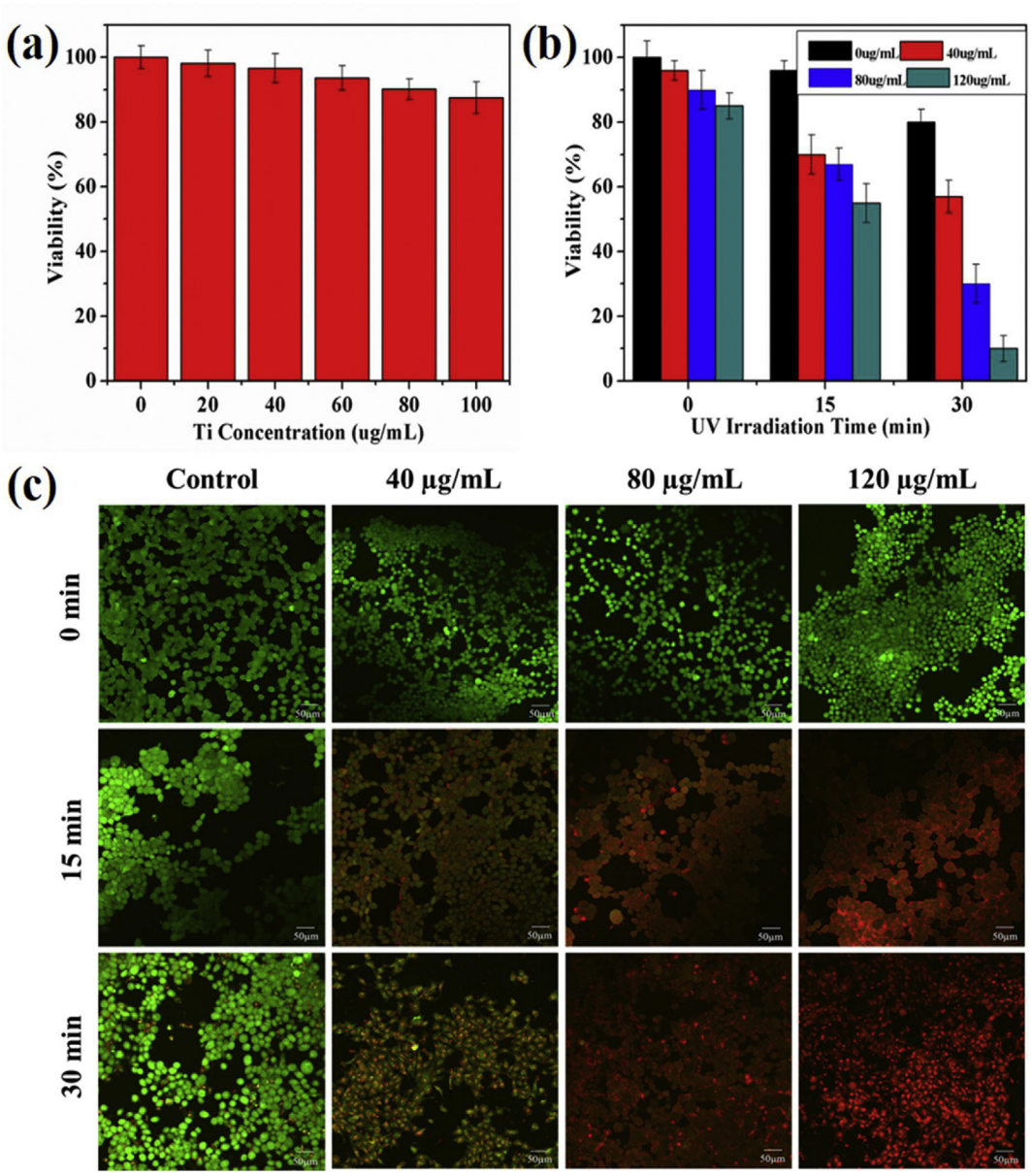

Fig. 6. Cell viability assay of Ag-TiO_2 HNRs by methyl thiazolyl tetrazolium (MTT) assay. (a) Cytotoxicity of Ag-TiO_2 HNRs was examined by incubating 4T1 breast cancer cells with HNRs in 0, 20, 40, 60, 80, and 100 μg/mL concentrations of Ti for 24 h. (b) 4T1 breast cancer cell viability of HNRs analyzed with various concentrations of Ti after UV light irradiation. (c) CLSM images of PI and Calcein-AM double-stained 4T1 cells under UV irradiation (scale bar is 50 μm).

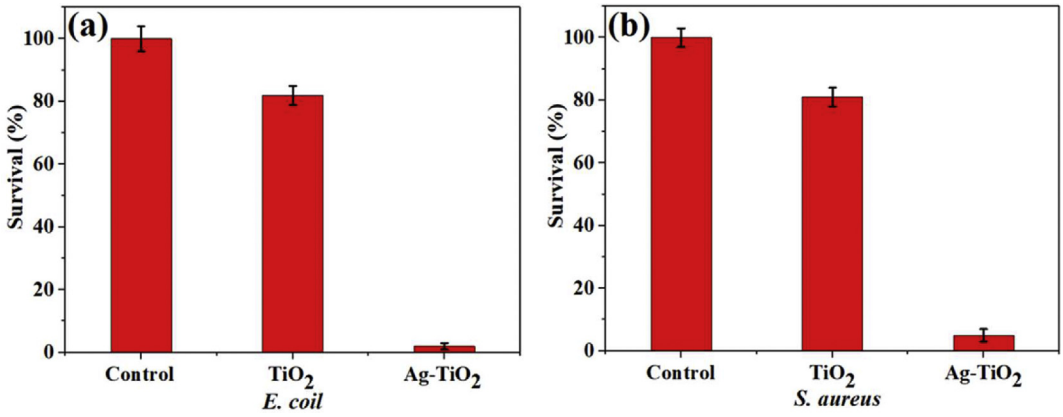

Fig. 7. Antibacterial activity of 6-h incubated with TiO_2 NRs and Ag-TiO_2 HNRs against (**a**) *Escherichia coli*, and (**b**) *Staphylococcus aureus* at 600 nm.

4. Conclusion

Biocompatible Ag-TiO_2 hybrid nanorods were designed with high ROS generation ability for enhanced photodynamic therapy and antimicrobial applications. A facile hydrothermal method was used to prepare the TiO_2 nanorods, and then a thermal decomposition technique was employed to grow the Ag (~4~5 nm) nanoparticles onto the TiO_2 (length = 35 ± 5 nm and width = 13 ± 2 nm) surface by a de-wetting process. The biocompatibility and aqueous dispersion capability of Ag-TiO_2 HNRs were further improved by the FDA-approved PF-127 amphiphilic copolymer and negligible toxicity effects were observed. Owing to their ultra-small size and hybrid nature, the prepared nanocomposites efficiently accumulated in the 4T1 cancer cells and possessed remarkable ROS generation to ablate tumor cells investigated by DPBF (ROS quencher). As an auspicious photosensitizer for phototherapy, Ag-TiO_2@PF-127 HNRs demonstrated excellent photodynamic suppression effects on 4T1 cancerous cells under a very low dose (5.6 mW/cm^2) of UV. In addition, Ag-TiO_2 HNRs showed significant antibacterial activity against *E. coli* and gram-positive *S. aureus* bacterial strains as compared with TiO_2 NPs, which is owed to the synergistic properties of Ag NPs and TiO_2 NRs. As shown in this comprehensive study, biocompatible Ag-TiO_2@PF-127 HNRs may serve as a new promising photo-activated nanomaterial with applications in photodynamic cancer therapy.

Declaration of competing interest

The authors declare that they have no known competing financial interests or personal relationships that could have appeared to influence the work reported in this paper.

Acknowledgements

The authors acknowledge the support of the National Natural Science Foundation of China (81950410638), Key Research and Development Program of Zhejiang Province (2021C01180) and Zhejiang International Science and Technology Cooperation Project (2019C04020).

Appendix A. Supplementary data

Supplementary data to this article can be found online at https://doi.org/10.1016/j.jsamd.2022.100417.

References

[1] Z. Liu, Z. Xie, W. Li, X. Wu, X. Jiang, G. Li, L. Cao, D. Zhang, Q. Wang, P. Xue, H. Zhang, Photodynamic immunotherapy of cancers based on nanotechnology: recent advances and future challenges, J. Nanobiotechnol. 19 (2021), 160, https://doi.org/10.1186/s12951-021-00903-7.

[2] M. Zhao, M. Xie, J. Guo, W. Feng, Y. Xu, X. Liu, S. Liu, Q. Zhao, Facile phototherapeutic nanoplatform by integrating a multifunctional polymer and MnO_2 for enhancing tumor synergistic therapy, Adv. Healthc. Mater. 8 (2019), 1900414, https://doi.org/10.1002/adhm.201900414.

[3] X. Deng, Z. Shao, Y. Zhao, Solutions to the drawbacks of photothermal and photodynamic cancer therapy, Adv. Sci. 8 (2021), 2002504, https://doi.org/10.1002/advs.202002504.

[4] A. Mahmood, A. Irfan, J.-L. Wang, Developing efficient small molecule acceptors with sp2-hybridized nitrogen at different positions by density functional theory calculations, molecular dynamics simulations and machine learning, Chem. Eur J. (2021), https://doi.org/10.1002/chem.202103712 n/a.

[5] D. Ziental, B. Czarczynska-Goslinska, D.T. Mlynarczyk, A. Glowacka-Sobotta, B. Stanisz, T. Goslinski, L. Sobotta, Titanium dioxide nanoparticles: prospects and applications in medicine, Nanomaterials 10 (2020) 387.

[6] D. Beydoun, R. Amal, G. Low, S. McEvoy, Role of nanoparticles in photocatalysis, J. Nanoparticle Res. 1 (1999) 439–458, https://doi.org/10.1023/A:1010044830871.

[7] Q. Wu, M. Liu, Z. Wu, Y. Li, L. Piao, Is photooxidation activity of {001} facets truly lower than that of {101} facets for anatase TiO_2 crystals? J. Phys. Chem. C 116 (2012) 26800–26804, https://doi.org/10.1021/jp3087495.

[8] Z. Tan, K. Sato, S. Takami, C. Numako, M. Umetsu, K. Soga, M. Nakayama, R. Sasaki, T. Tanaka, C. Ogino, A. Kondo, K. Yamamoto, T. Hashishin, S. Ohara, Particle size for photocatalytic activity of anatase TiO_2 nanosheets with highly exposed {001} facets, RSC Adv. 3 (2013) 19268–19271, https://doi.org/10.1039/C3RA43383H.

[9] C. Dette, M.A. Pérez-Osorio, C.S. Kley, P. Punke, C.E. Patrick, P. Jacobson, F. Giustino, S.J. Jung, K. Kern, TiO_2 anatase with a bandgap in the visible region, Nano Lett. 14 (2014) 6533–6538, https://doi.org/10.1021/nl503131s.

[10] V. Mishra, M.K. Warshi, A. Sati, A. Kumar, V. Mishra, R. Kumar, P.R. Sagdeo, Investigation of temperature-dependent optical properties of TiO_2 using diffuse reflectance spectroscopy, SN Appl. Sci. 1 (2019), 241, https://doi.org/10.1007/s42452-019-0253-6.

[11] B. Wu, W.Q. Zhuang, M. Sahu, P. Biswas, Y.J. Tang, Cu-doped TiO(2) nanoparticles enhance survival of Shewanella oneidensis MR-1 under ultraviolet light (UV) exposure, Sci. Total Environ. 409 (2011) 4635–4639, https://doi.org/10.1016/j.scitotenv.2011.07.037.

[12] R. Zhao, J. Cao, X. Yang, Q. Zhang, M.Z. Iqbal, J. Lu, X. Kong, Inorganic material based macrophage regulation for cancer therapy: basic concepts and recent advances, Biomater. Sci. 9 (2021) 4568–4590, https://doi.org/10.1039/D1BM00508A.

[13] Z. Hou, Y. Zhang, K. Deng, Y. Chen, X. Li, X. Deng, Z. Cheng, H. Lian, C. Li, J. Lin, UV-emitting upconversion-based TiO_2 photosensitizing nanoplatform: near-infrared light mediated in vivo photodynamic therapy via mitochondria-involved apoptosis pathway, ACS Nano 9 (2015) 2584–2599, https://doi.org/10.1021/nn506107c.

[14] J. Wang, S. Qu, Z. Zhong, S. Wang, K. Liu, A. Hu, Fabrication of TiO_2 nanoparticles/nanorod composite arrays via a two-step method for efficient dye-sensitized solar cells, Prog. Nat. Sci.: Mater. Int. 24 (2014) 588–592, https://doi.org/10.1016/j.pnsc.2014.10.013.

[15] C. Yu, J. Zhang, H. Yang, L. Zhang, Y. Gao, Enhanced photovoltaic conversion efficiency of a dye-sensitized solar cell based on TiO_2 nanoparticle/nanorod array composites, J. Mater. Res. 34 (2019) 1155–1166, https://doi.org/10.1557/jmr.2018.420.

[16] L. Wang, C. Hu, L. Shao, The antimicrobial activity of nanoparticles: present situation and prospects for the future, Int. J. Nanomed. 12 (2017) 1227–1249, https://doi.org/10.2147/ijn.S121956.

[17] A. Baranwal, A. Srivastava, P. Kumar, V.K. Bajpai, P.K. Maurya, P. Chandra, Prospects of nanostructure materials and their composites as antimicrobial agents, Front. Microbiol. 9 (2018), https://doi.org/10.3389/fmicb.2018.00422.

[18] X.-L. Hu, Y. Shang, K.-C. Yan, A.C. Sedgwick, H.-Q. Gan, G.-R. Chen, X.-P. He, T.D. James, D. Chen, Low-dimensional nanomaterials for antibacterial applications, J. Mater. Chem. B 9 (2021) 3640–3661, https://doi.org/10.1039/D1TB00033K.

[19] Z. Zhang, W. Shen, J. Xue, Y. Liu, Y. Liu, P. Yan, J. Liu, J. Tang, Recent advances in synthetic methods and applications of silver nanostructures, Nanoscale Res. Lett. 13 (2018), 54, https://doi.org/10.1186/s11671-018-2450-4.

[20] L. Zhang, Q. Cheng, C. Li, X. Zeng, X.-Z. Zhang, Near infrared light-triggered metal ion and photodynamic therapy based on AgNPs/porphyrinic MOFs for tumors and pathogens elimination, Biomaterials 248 (2020), 120029, https://doi.org/10.1016/j.biomaterials.2020.120029.

[21] X. Fan, L. Yahia, E. Sacher, Antimicrobial properties of the Ag, Cu nanoparticle System, Biology 10 (2021), https://doi.org/10.3390/biology10020137.

[22] K. Arkusz, E. Paradowska, M. Nycz, J. Mazurek-Popczyk, K. Baldy-Chudzik, Evaluation of the antibacterial activity of Ag- and Au-nanoparticles loaded TiO_2 nanotubes, J. Biomed. Nanotechnol. 16 (2020) 1416–1425, https://doi.org/10.1166/jbn.2020.2979.

[23] J. Helmlinger, C. Sengstock, C. Groß-Heitfeld, C. Mayer, T.A. Schildhauer, M. Köller, M. Epple, Silver nanoparticles with different size and shape: equal cytotoxicity, but different antibacterial effects, RSC Adv. 6 (2016) 18490–18501, https://doi.org/10.1039/C5RA27836H.

[24] M.Z. Iqbal, W. Ren, M. Saeed, T. Chen, X. Ma, X. Yu, J. Zhang, L. Zhang, A. Li, A. Wu, A facile fabrication route for binary transition metal oxide-based Janus nanoparticles for cancer theranostic applications, Nano Res. 11 (2018) 5735–5750, https://doi.org/10.1007/s12274-017-1628-x.

[25] M.Z. Iqbal, D. Luo, O.U. Akakuru, A. Mushtaq, Y. Hou, I. Ali, G. Ijaz, B. Khalid, X. Kong, A. Wu, Facile synthesis of biocompatible magnetic titania nanorods for T1-magnetic resonance imaging and enhanced phototherapy of cancers, J. Mater. Chem. B 9 (2021) 6623–6633, https://doi.org/10.1039/D1TB01097B.

[26] A. Mushtaq, Y. Hou, C. Tian, T. Deng, C. Xu, Z. Sun, X. Kong, M. Zubair Iqbal, Facile synthesis of Mn doped TiO_2 rhombic nanocomposites for enhanced T_1-Magnetic resonance imaging and photodynamic therapy, Mater. Res. Bull. 144 (2021), 111481, https://doi.org/10.1016/j.materresbull.2021.111481.

[27] W. Zhang, Z. Jiang, L. Hao, G. Lu, Y. Ni, C. Lu, Z. Xu, Three-dimensional ordered macroporous nano-architecture and its enhancing effects on Raman detection sensitivity for Eosin Y molecules, Mater. Des. 119 (2017) 456–463, https://doi.org/10.1016/j.matdes.2017.01.090.

[28] H.E. Chao, Y.U. Yun, H.U. Xingfang, A. Larbot, Effect of silver doping on the phase transformation and grain growth of sol-gel titania powder, J. Eur. Ceram. Soc. 23 (2003) 1457–1464, https://doi.org/10.1016/S0955-2219(02)00356-4.

[29] R. Lu, J. Sha, W. Xia, Y. Fang, L. Gu, Y. Wang, A 3D-SERS substrate with high stability: silicon nanowire arrays decorated by silver nanoparticles, CrystEngComm 15 (2013) 6207–6212, https://doi.org/10.1039/C3CE40788H.

[30] D. Wu, J. Ma, Y. Bao, W. Cui, T. Hu, J. Yang, Y. Bai, Fabrication of porous Ag/TiO_2/Au coatings with excellent multipactor suppression, Sci. Rep. 7 (2017), 43749, https://doi.org/10.1038/srep43749.

[31] B. Wang, X. Li, S. Liang, R. Chu, D. Zhang, H. Chen, M. Wang, S. Zhou, W. Chen, X. Cao, W. Feng, Adsorption and oxidation of SO_2 on the surface of TiO_2 nanoparticles: the role of terminal hydroxyl and oxygen vacancy−Ti3+ states, Phys. Chem. Chem. Phys. 22 (2020) 9943−9953, https://doi.org/10.1039/D0CP00785D.

[32] J. Xu, Z. Wang, W. Li, X. Zhang, D. He, X. Xiao, Ag nanoparticles located on three-dimensional pine tree-like hierarchical TiO_2 nanotube Array films as high-efficiency plasmonic photocatalysts, Nanoscale Res. Lett. 12 (2017), 54, https://doi.org/10.1186/s11671-017-1834-1.

[33] M. Sun, B. Sun, Y. Liu, Q.-D. Shen, S. Jiang, Dual-color fluorescence imaging of magnetic nanoparticles in live cancer cells using conjugated polymer probes, Sci. Rep. 6 (2016), 22368, https://doi.org/10.1038/srep22368.

[34] P. Sudhindra, S. Ajay Sharma, N. Roy, P. Moharana, P. Paira, Recent advances in cytotoxicity, cellular uptake and mechanism of action of ruthenium metallodrugs: a review, Polyhedron 192 (2020), 114827, https://doi.org/10.1016/j.poly.2020.114827.

[35] J. Zhao, M.H. Stenzel, Entry of nanoparticles into cells: the importance of nanoparticle properties, Polym. Chem. 9 (2018) 259−272, https://doi.org/10.1039/C7PY01603D.

[36] A. Nsubuga, G.A. Mandl, J.A. Capobianco, Investigating the reactive oxygen species production of Rose Bengal and Merocyanine 540-loaded radioluminescent nanoparticles, Nanoscale Adv. 3 (2021) 1375−1381, https://doi.org/10.1039/D0NA00964D.

[37] I. Zada, W. Zhang, W. Zheng, Y. Zhu, Z. Zhang, J. Zhang, M. Imtiaz, W. Abbas, D. Zhang, The highly efficient photocatalytic and light harvesting property of Ag-TiO_2 with negative nano-holes structure inspired from cicada wings, Sci. Rep. 7 (2017), 17277, https://doi.org/10.1038/s41598-017-17479-8.

[38] K. Gupta, R.P. Singh, A. Pandey, A. Pandey, Photocatalytic antibacterial performance of TiO_2 and Ag-doped TiO_2 against S. aureus. P. aeruginosa and E. coli, Beilstein J. Nanotechnol. 4 (2013) 345−351, https://doi.org/10.3762/bjnano.4.40.

[39] K. Gupta, R.P. Singh, A. Pandey, A. Pandey, Correction: photocatalytic antibacterial performance of TiO_2 and Ag-doped TiO_2 against S. aureus. P. aeruginosa and E. coli, Beilstein J. Nanotechnol. 11 (2020) 547−549, https://doi.org/10.3762/bjnano.11.43.